ACS APPLIED MATERIALS & INTERFACES

Research Article

www.acsami.org

Sulfur, Trace Nitrogen and Iron Codoped Hierarchically Porous Carbon Foams as Synergistic Catalysts for Oxygen Reduction Reaction

Zhaoyan Guo,[†] Congcong Jiang,[†] Chao Teng,[†] Guangyuan Ren,[†] Ying Zhu,*[,†] and Lei Jiang[‡]

[†]Key Laboratory of Bio-inspired Smart Interfacial Science and Technology of Ministry of Education, School of Chemistry and Environment, Beihang University, Beijing 100191, People's Republic of China

[‡]Beijing National Laboratory for Molecular Sciences, Institute of Chemistry, Chinese Academy of Sciences, Beijing 100190, People's Republic of China

Supporting Information

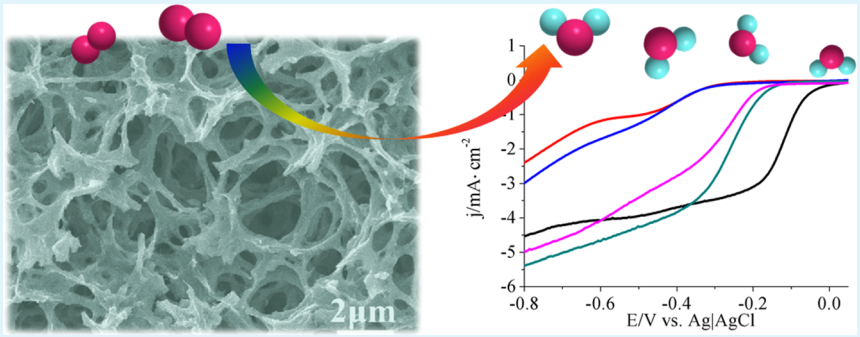

ABSTRACT: Sulfur, trace nitrogen and iron codoped, hierarchically porous carbon foams (HPCFs) were fabricated by directly pyrolyzing sulfur-enriched conductive polymer, poly(3,4-ethylenedioxythiphene)−polystyrenesulfonic acid (PEDOT-PSS) aerogels under argon atmosphere. This simple pyrolysis treatment results in the molecular rearrangement of heteroatom sulfur, adjacent carbons and trace nitrogen/iron from oxidants to form active catalytic sites of HPCFs. At the same time, the high porosity of HPCFs provides the large surface area for the uniform distribution of active sites, and allows rapid oxygen transport and diffusion. As a result, these HPCFs exhibit the enhanced catalytic performances for oxygen reduction reaction (ORR) via a direct four-electron reduction pathway in alkaline electrolyte. Besides, they also display a higher stability and better methanol/CO tolerance than the commercial Pt/C catalyst, which makes them promising low cost, non-precious-metal ORR catalysts for practical application in fuel cells and metal−air batteries.

KEYWORDS: *hierarchically porous structures, heteroatoms codoped carbon foams, oxygen reduction electrocatalysts, synergistic effect*

INTRODUCTION

The sluggish kinetics of the cathodic oxygen reduction reaction (ORR) is the primary limiting factor in the energy conversion efficiency of fuel cells and metal−air batteries.[1] Although Pt-based catalysts have been universally researched and recognized as the most effective ORR catalysts in improving the reaction velocity, they still suffer from the drawbacks of high cost, poor long-term stability and methanol/CO poisoning effects.[2,3] Thus, much effort has been devoted to developing low cost, non-precious-metal catalysts with the improved catalytic efficiency, durability and antipoisoning ability. Recently, heteroatoms doping has been promoted as a promising route to improve the catalytic performances of various materials. For example, Huang et al. have shown that Ce and F or Gd doped Bi_2WO_6 can exhibit increased photocatalytic activities for the degradation of rhodamine B (RhB) and generation of photocurrent under visible light irradiation.[4−6] Especially, as one of the most promising electrocatalysts toward ORR, heteroatoms doped carbon materials, including nitrogen (N), phosphor (P), boron (B) or sulfur (S) doped carbon nanotubes/graphene,[7−9] exhibited not only efficient ORR catalytic performances but also higher stability and much better resistance to CO/methanol poisoning than commercial Pt/C catalysts. To date, it has been demonstrated that the difference in electronegativity between N/P/B and C in graphitic framework usually create the charged sites on adjacent carbon framework to facilitate the oxygen reduction process.[9,10] Whereas, S that has electronegativity similar to carbon was also implanted in the carbon backbone for enhancing electrocatalytic activity due to the electrical effect of spin density.[9,11] Nowadays, although there have also been studies on codoped carbon nanomaterials with two elements of different

Received: September 19, 2014
Accepted: November 17, 2014
Published: November 17, 2014

electronegativity presenting outstanding capacity in ORR,[7,12−14] it is still desirable but challenging to produce this kind of catalysts with high-surface-density active sites and access to oxygen gas at the same time.[15−17]

For decades, the nanostructured conducting polymers, including polyaniline (PANI), polypyrrole (PPy), poly(3,4-ethylenedioxythiphene) (PEDOT), have aroused much attention in both fundamental research and various applications.[18−20] They are expected to display excellent performance in energy conversion/storage devices because of their unique properties arising from high electrical conductivity, large surface area, short path lengths for the transport of ions and high electrochemical activities.[18,21−23] Our previous work has shown that micro/nanostructured PEDOT can be developed as efficient ORR electrocatalysts in their own, exhibiting high performance and better durability than the precious Pt catalyst in a wide pH range.[24,25] Besides, PANI and PPy, with intrinsic nitrogen-containing units, have been researched to prepare high-performance, nitrogen-doped ORR catalysts through a simple annealing process.[26,27] Recently, conductive polymer aerogels, showing their three-dimensional, highly interconnected and porous structures, were easily synthesized in large scale through chemical polymerization methods,[28−31] which may use them as candidate precursors for heteroatom-doped carbon materials with high surface areas toward ORR.[32]

Herein, we fabricate S, trace N and Fe codoped, hierarchically porous carbon foams (HPCFs) as effective ORR electrocatalysts by pyrolyzing poly(3,4-ethylenedioxythiphene)-polystyrenesulfonic acid (PEDOT-PSS) aerogels at temperatures of 700, 800 and 900 °C (nominated as HPCF-700, HPCF-800 and HPCF-900) under argon atmosphere. PEDOT-PSS aerogels are employed as the sulfur-enriched precursor for the reason that both PEDOT and PSS possess one sulfur atom in per repeat unit, respectively (Scheme 1 in the Supporting Information). The oxidant residues, $Fe(NO_3)_3$, can function as the sources of trace nitrogen and iron that work together with sulfur dopants to create synergistic effects for ORR catalytic process. Besides, the hierarchically micro/nanostructures of PEDOT-PSS aerogels have highly porous features, which can provide relatively large surface area favorable to the distribution of catalytic active sites, and the mass transport, adsorption and reduction of oxygen during the ORR process. It is envisaged that HPCFs displayed the high ORR electrocatalytic activities via a direct four-electron pathway, which should be due to the synergistic effect derived from the S, trace N and Fe codoping, and the hierarchically porous structures. Moreover, HPCFs electrocatalysts showed the good long-term operation stability and excellent CO and methanol tolerance than commercial Pt/C catalysts, which may make them promising Pt/C alternatives as ORR electrocatalysts for application in fuel cell technology.

EXPERIMENTAL SECTION

Reagents and Materials. $Fe(NO_3)_3{\cdot}9H_2O$, KOH of analytical grade was obtained from Beijing Chemical Reagent Co. Int. and used without further purification. 3,4-Ethylenedioxythiophene (EDOT) was purchased from TCI and used distilled under reduced pressure prior to use. Poly(sodium 4-styrenesulfonate) (NaPSS, Mw 70 000) was bought from Sigma-Aldrich. Nafion (DuPont, 10 wt %) was diluted to 0.05 wt % by ethanol. The commercial Pt/C (20 wt %) catalysts were purchased from the Johnson Matthey Company.

Preparation of HPCFs. Porous PEDOT-PSS gels were fabricated, according to a previous report.[33] The composites were dialyzed against deionized water for 24 h to remove excess oxidant and dried in a vacuum at room temperature for 48 h. Then the purified PEDOT-PSS were pyrolyzed under an argon atmosphere at different annealing temperatures of 700, 800 and 900 °C for 2 h; thus, the products are denoted as HPCF-700, HPCF-800 and HPCF-900, respectively.

Materials Characterization. The morphology of the PEDOT-PSS aerogels and HPCFs was measured by field emission scanning electron microscopy (FESEM, JEOL7500). Molecular structures of the polymerized products were characterized by X-ray photoelectron spectroscopy (XPS) and Raman spectra. XPS spectra of the as-synthesized PEDOT pressed pellet and HPCFs were conducted on a VG ESCALAB 220i-XL instrument with a monochromatic Al Kα X-ray source. Raman spectra were recorded on a Jobin Yvon (Laboratory RAM HR1800) confocal mocro-Raman spectrometer backscattered geometry through a 10 × (NA = 0.25) microscope objective. an Ar+ laser emitting at a wavelength of 514.5 nm was used as a source of excitation. Nitrogen sorption/desorption measurements were performed with ASAP 2020M (Micromeritics, USA) to obtain BET-specific surface area and pore size pore size distribution. Thermogravimetric analysis (TGA) was carried out using a STA449F3 (NETZSCH) analyzer. The temperature range is between 40 and 900 °C at a heating rate of 10 °C min^{-1} under an argon atmosphere.

Electrochemical Characterization. The electrochemical characterization for ORR was conducted on a computer-controlled electrochemical station (CHI 760D, Shanghai) with a standard three-electrode cell system equipped with gas flow system. A platinum wire was used as the counter electrodes and a saturated Ag|AgCl (KCl sat.) as the reference electrode. The working electrodes were prepared by applying the catalyst ink onto a prepolished glass carbon disk electrode (GC). Briefly, the catalyst was dispersed in ethanol and ultrasonicated for 20 min to form a uniform catalyst ink (2 mg mL^{-1}). Then 15 μL of catalyst ink was applied on the GC electrode (5 mm in diameter). After the material dried at room temperature, 5 μL of Nafion (0.05 wt %) solution in ethanol was applied on the surface of the catalyst layer to form a thin protective film. The electrolyte for ORR was 0.1 M aqueous KOH, which was saturated with oxygen or nitrogen for 20 min prior to the electrochemical tests. The ORR activity was evaluated by cyclic voltammetry (CV) and linear sweep voltammetry (LSV) techniques on a rotating disk electrode (RDE) in O_2-saturated 0.1 M KOH solutions. Methanol crossover, CO poisoning and durability tests were conducted by a chronoamperometric technique at the bias potential of −0.3 V (vs Ag/AgCl) in O_2-saturated 0.1 M KOH solutions with a rotation rate of 800 rpm.

RESULTS AND DISCUSSION

The PEDOT-PSS aerogels were first fabricated by chemical oxidative polymerization of 3,4-ethylenedioxythiophene (EDOT), in the presence of $Fe(NO_3)_3$ as an oxidant and cross-linking agent, as reported previously.[33] The FESEM images of as-prepared PEDOT-PSS aerogels are shown in Figure 1a,b, indicating that the as-fabricated PEDOT-PSS aerogels exhibit rich hierarchical pores with a wide size distribution ranging from about 400 nm to 1 μm in diameter. The solid walls of the pores are randomly self-assembled by intertwisted nanofibers of PEDOT-PSS, whose diameters are in the range of several hundred nanometers. A magnified SEM image of PEDOT-PSS aerogels (Figure 1b) demonstrates that the surface of solid wall initially constitutes of rough textures. After pyrolysis under argon at 800 °C, HPCF-800 still displays the hierarchically porous structures that are nearly identical to that of the PEDOT-PSS aerogel precursor, while the surface of their solid wall shows many well-formed mesopores, as shown in Figure 1c,d. This phenomenon should be attributable to the chemical decomposition of PEDOT-PSS caused by high temperature. Like HPCF-800, moreover, the HPCF-700 and HPCF-900 also displayed the hierarchical microporous/mesoporous structures (Figure S1, Supporting Information),

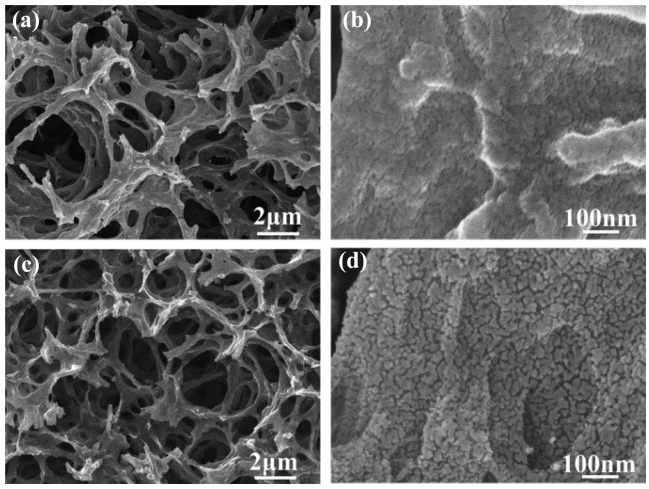

Figure 1. SEM images of as-prepared PEDOT-PSS aerogels (a, b) and HPCF-800 (c, d).

while HPCF-900 shows nanoparticles aggregation on the surfaces (Figure S1c,d, Supporting Information). These results indicate that pyrolysis temperatures played a pivotal role in forming microscopic structures of the products. Nitrogen physisorption isotherms were measured to further investigate the porous nature of HPCFs, as shown in Figure S2 (Supporting Information). The Brunauer–Emmett–Teller (BET) surface areas are 354.4, 370.4 and 453.6 m^2 g^{-1} for HPCF-700, HPCF-800 and HPCF-900, respectively, which are much higher than that of as-prepared PEDOT-PSS aerogel (38.3 m^2 g^{-1}), thus indicating a significant improvement in mass transport of oxygen. The corresponding pore size distribution curves calculated from the desorptionbranches of the isotherms by the Barrett–Joyner–Halenda (BJH) model for all samples were shown in Figure S2 (Supporting Information). The curve of PEDOT-PSS shows a broad pore size distribution ranging from 6 to 40 nm. However, after pyrolysis, it is worth noting that new, narrow pore size distributions appear for all HPCFs. The sharp, strong peaks are at around 3.8 nm for HPCF-700, 4.1 nm for HPCF-800 and 4.0 nm for HPCF-900, respectively. Besides, the original broad pore size distributions among 6–40 nm were also kept for all HPCFs, but the relative peak intensities of them decrease sharply with the increasing pyrolysis temperature, especially for HPCF-700 and HPCF-800. Thus, a higher BET surface area of HPCF-800 than HPCF-700 can be seen. More importantly, the enhancement of surface areas and hierarchically porous structures of HPCFs are beneficial for the increase of active sites on catalyst surfaces.

The molecular structures and surface chemical compositions of as-prepared PEDOT-PSS aerogel and HPCFs were investigated using Raman spectroscopy and X-ray photoelectron spectroscopy (XPS). The Raman spectrum of the as-prepared PEDOT-PSS aerogel shows a strong vibration band between 1300 and 1520 cm^{-1} should be contributed to the stretching vibration of $C_\alpha{=}C_\beta$ on the five-membered thiophene ring of the PEDOT chains (Figure 2a).[34] After pyrolysis, the Raman spectra of HPCFs, including HPCF-700, HPCF-800 and HPCF-900, show two feature peaks of graphite: the G peak centered at 1580 cm^{-1} is due to the bond stretching of all pairs of sp^2 atoms in both rings and chains, whereas the D peak centered at 1360 cm^{-1} is attributable to the breathing modes of sp^3 atoms in rings (Figure 2a).[35] The ratios of

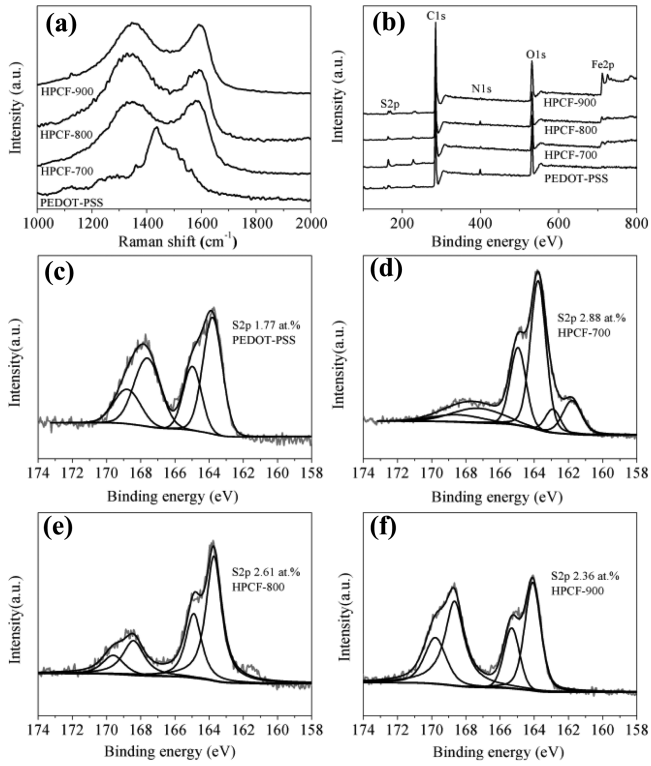

Figure 2. (a) Raman and (b) XPS survey spectra of PEDOT-PSS aerogels, HPCF-700, HPCF-800 and HPCF-900. (c–f) High resolution S 2p spectra of PEDOT-PSS aerogels, HPCF-700, HPCF-800 and HPCF-900.

integrated intensity of the D and G band (I_D/I_G) ratios is widely used to assess the density of defects in graphite materials. It is observed that the I_D/I_G values are 1.20 for HPCF-700, 1.19 for HPCF-800 and 1.18 for HPCF-900, respectively, indicating that the graphitization degrees of HPCFs are improved with the increasing temperatures. Thus, it is deduced that the PEDOT-PSS aerogels undergo a carbonization transformation through pyrolysis process at high-temperature. XPS analysis that is more sensitive to the surface chemical compositions was employed to get further information on HPCF-700, HPCF-800 and HPCF-900. As shown in Figure 2b and Table S1 (Supporting Information), all samples have the elements of C, O, S, as well as a trace N and Fe. Among them, the C (79.34 at. %), O (18.31 at. %) and S (1.77 at. %) atoms mainly originate from PEDOT-PSS, while trace N (0.31 at. %) and Fe (0.27 at. %) elements are from the residual oxidant of $Fe(NO_3)_3$ after the chemical polymerization of EDOT. After pyrolysis, the contents of S has changed from 1.77 at. % for PEDOT-PSS to 2.88, 2.61 and 2.36 at. % with respect to HPCF-700, HPCF-800 and HPCF-900, respectively. However, the S contents of HPCFs are higher than that of PEDOT-PSS. The reason is that more S elements may come close to surface of the materials, and the decomposition of the oxygen-containing groups lead to an increase of relative S contents. The relative contents of N decrease gradually from 0.27 at. % for HPCF-700 to 0.21 at. % for HPCF-800 and 0.18 at. % for HPCF-900 with the ascending pyrolysis temperatures. At the same time, the relative contents of Fe declines slightly along with temperature ascension and are 0.24 at. % for HPCF-700, 0.13 at. % HPCF-800 and 0.11 at. % for HPCF-900. The high resolution C 1s spectra of the HPCF-s reveal the

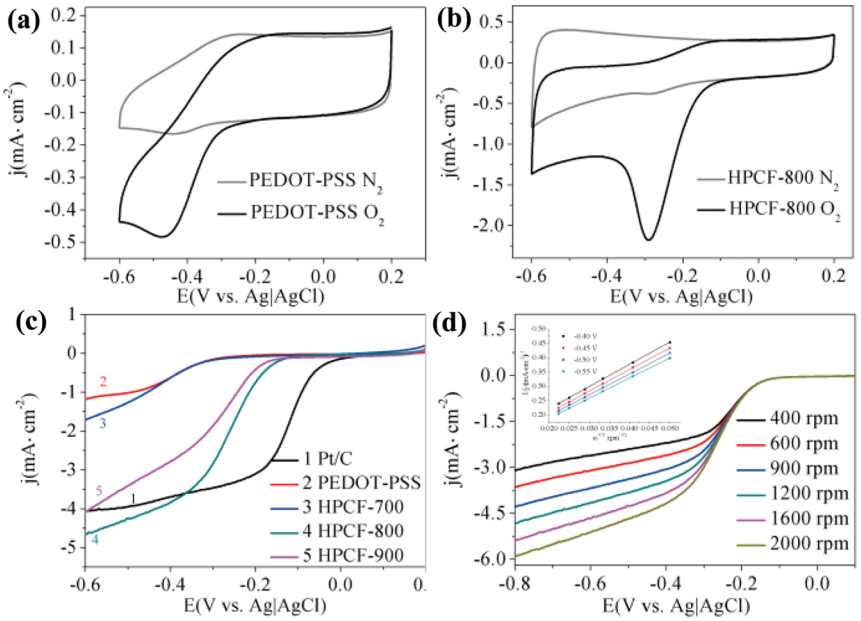

Figure 3. Cyclic voltagrammetry (CV) curves of (a) PEDOT−PSS and (b) HPCF-800 in N_2 (gray lines) or O_2 (black lines) saturated 0.1 M KOH solutions. The sweep rate is 50 mV·s^{-1}. (c) Linear sweep voltammetry (LSV) curves of commercial Pt/C, HPCF-700, HPCF-800 and HPCF-900 catalysts on a glassy carbon rotating disk electrode (RDE) in O_2-saturated 0.1 M KOH solutions at the scan rate of 10 mV·s^{-1} with the rotation speed of 1600 rpm. (d) The LSV curves of HPCF-800 at different rotation speed in the O_2-saturated 0.1 M KOH solution at the scan rate of 10 mV·s^{-1}. Inset: K-L plots of HPCF-800 catalyst.

dominant contribution of sp^3 and sp^2 hybrids at 285.1 and 284.5 eV after pyrolysis in accordance with the result of Raman analysis, and are different from the C−C bonds in the polymer chains of the PEDOT-PSS (Figure S3, Supporting Information). The characteristic peaks of C−S bonds in HPCFs are found at 286.4 eV, a little higher than that in PEDOT-PSS (285.9 eV), which indicates the chemical rearrangements of C−S bonds after pyrolysis.[36] For further analysis, the high resolution S 2p XPS spectra are shown in Figure 2c−f, all of which come from the spin−orbit coupling, S $2p_{3/2}$ and S $2p_{1/2}$ with 1.2 eV energy splitting and 1:2 intensity ratio. For PEDOT-PSS, S 2p core levels show two doublets at 163.8/165.0 and 167.6/168.8 eV originated from thiophene sulfur in PEDOT and sulfonated groups in PSS, respectively.[29] After pyrolysis, however, the spectra of HPCFs show that the peaks at binding energies of 163.6/164.8 eV should be attributable to S−S bonds between two aromatic rings, according to previous reports.[36,37] Moreover, the peaks among the higher binding energies of 167.3−169.8 eV should be attributed to sulfonated aromatic systems in the form of -C−SO_2−C-.[38] Whereas, the new peaks at 162.9 and 161.7 eV appeared in the XPS fitting curves of S 2p for HPCF-700, should be attributed to S−H bonds.[11] The high resolution N 1s spectra of HPCFs are given in Figure S4 (Supporting Information). HPCF-700 displays two peaks centered at 400.3 and 399.6 eV, indicating that nitrogen can dope into the carbon as quaternary-N and pyrrolic-N. As for HPCF-800, the newly appeared peak at 399.3 eV should be due to pyridinic-N. Three peaks at 401.7, 400.5 and 399.6 in the spectrum of HPCF-900 should be attributed to high-oxidation states of nitrogen atoms, protonated nitrogen atoms and pyrrolic-N, respectively. It is generally accepted that quaternary-N and pyridinic-N are considered as the electrocatalytic active sites for ORR in nitrogen-doped carbon (Figure S4, Supporting Information).[26] Moreover, the detailed information on high resolution O 1s and Fe 2p XPS spectra is also given in Figures S5 and S6 (Supporting Information). The presence of O is possible due to the residual oxygen-containing groups in precursors. And Fe 2p HPCFs can be deconvoluted into two peaks at 710.9/724.5 eV, corresponding to Fe_2O_3 formed high-temperature treatment. Taken together, it can thus be concluded that, the anoxic pyrolysis process make sulfur and trace nitrogen/iron doped into carbon framework, thus leading to the formation C−S and C−N bonds acted as catalytic active sites. The thermogravimetric analysis (TGA) was employed to further investigate the physical changing and chemical reactions during the pyrolysis of PEDOT-PSS. As shown in Figure S7 (Supporting Information), one can observe a small decay beginning from 40 to 320 °C corresponding to the evaporation of solvent molecules that were trapped on the cross-linked PEDOT-PSS chains. The second weight loss step, which takes place in the temperature range of 320−900 °C, corresponds to the decomposition process of polymer backbone with a weight yield of 40%. Moreover, three subsequent decomposition decays were observed at 390, 480 and 600 °C, which is due to the presence of different compositions in the polymeric bases.[39,40]

To evaluate the ORR electrocatalytic activities of PEDOT-PSS and HPCFs, the cyclic voltammetry (CV) tests were performed in N_2- and O_2-saturated 0.1 mol L^{-1} KOH solution at a scan rate of 50 mV s^{-1}. From Figure 3a, it can be clearly seen that the as-prepared PEDOT-PSS aerogel exhibits ORR performances with the onset potential at −0.15 V and peak potential at −0.48 V with a maximum current density of 0.46 mA cm^{-2}, which is consistent with our previous report.[25] As a comparison, the HPCF-800 catalyst shows better catalytic performance than that of PEDOT-PSS aerogel, more positive onset potential at −0.1 V and peak potential at −0.31 V (Figure 3b). More importantly, the HPCF-800 catalyst gives a much higher catalytic current of 1.67 mA cm^{-2}, which is 3−4 times higher than that of the PEDOT-PSS aerogel. The CV curves of

HPCF-700 and HPCF-900 are also tested under identical conditions, and the peak reduction current densities are almost the same (0.7 mA cm^{-2}), which are inferior to that of HPCF-800 (Figure S8, Supporting Information).

The linear sweep voltagrammetry (LSV) curves of these catalysts are compared with the performance of commercial Pt/C under the rotation speed of 1600 rpm. As is shown in Figure 3c, the onset potential and half-wave potential of PEDOT-PSS is −0.25 and −0.71 V, respectively, with the limiting current density of 3.5 mA·cm^{-2}. For HPCF-700, the onset and half-wave potential are close to that of PEDOT-PSS, while the limiting current density is slightly larger. When pyrolysis temperature increases, the onset potentials of HPCF-800 and HPCF-900 shift positively to −0.14 and −0.16 V, and their half-wave potentials ascend to −0.30 and −0.34 V, respectively. Importantly, the limiting current density of HPCF-800 is close to that of commercial Pt/C. Consequently, these HPCFs, especially HPCF-800 and HPCF-900, having the relatively high onset potentials and limiting current densities can function as high-performance ORR catalyst, which could open up real opportunity for practical application in fuel cells and metal−air batteries. According to previously theoretical study, we proposed that the efficient electrocatalytic properties of HPCFs might be attributable to the molecular rearrangements of C−S moieties that act as effective catalytic sites for ORR, as well as a synergistic effect between sulfur and trace amount of nitrogen and iron. Moreover, the hierarchically porous structures of the foams can also provide large surface area and more active sites, as a result of which, absorption and reduction of oxygen molecules can be improved effectively.

To further investigate the ORR kinetics processes of HPCFs catalysts, LSVs were performed on a rotating disk electrode (RDE) under different rotation speeds. The transferred electron number (n) per oxygen molecule can be calculated by the Koutechy−Levich equation, as given below (eqs 1 and 2):

$$\frac{1}{j} = \frac{1}{j_k} + \frac{1}{B\omega^{0.5}} \quad (1)$$

$$B = 0.2nF(D_{O_2})^{2/3}\upsilon^{-1/6}C_{O_2} \quad (2)$$

where j_k is kinetic current and ω is rotating rate. B can be determined by the slope of K-L plots based on the Levich equation, where n, F, D_{O_2}, ν and C_{O_2} represent the transferred electron number per oxygen molecule, Faraday constant (96485 C·mol^{-1}), diffusion coefficient of O_2 (1.9×10^{-5} $cm^2 \cdot s^{-1}$), the kinetic viscosity (1.1×10^{-2} $cm^2 \cdot s^{-1}$) and the bulk concentration of O_2 (1.2×10^{-6} mol·cm^{-3}) in 0.1 M KOH solutions, respectively. The constant 0.2 is adopted when the rotation speed is expressed in rpm.

From Figure 3d, it can be seen that the diffusion current densities for HPCF-800 catalyst depend on the rotating rates, and thus a diffusion-controlled oxygen reduction reaction can be verified. Based on the Koutecky−Levich (K-L) equations (details in the Supporting Information) and K-L plots (Inset of Figure 3d), the transferred electrons number (n) in the reduction process is calculated to be 4.0 at −0.40 V for HPCF-800. The result indicates that the ORR catalyzed by HPCF-800 occurs almost entirely through the four-electron reduction pathway, close to that of commercial Pt/C. Although the n for PEDOT-PSS catalysts is 3.8 at −0.40 V, the LSV curves of PEDOT-PSS show two major plateau regions attributed to a two-step reduction mechanism at considerably negative potentials (Figure S9a,b, Supporting Information). As for HPCF-700, the n is 2.6 at −0.40 V, indicating a two-electron or a mixed reduction routine under potentials, as shown in Figure S9c,d, Supporting Information. The n of HPCF-900 is slightly lower than these of HPCF-800 (Figure S9e,f, Supporting Information), and n can reach 3.7 at −0.40 V, indicating an almost four-electron reduction pathway. Taken together, it can be concluded that HPCF-800 and HPCF-900 can exhibit superior ORR properties to that of HPCF-700. Although the exact mechanism is unknown now, combined with the XPS analyses, we can propose that these results were mainly attributed to the coordination of S, trace N and Fe dopants. Generally speaking, the high catalytic behavior of S-doped carbon is mostly determined by the spin density arisen from the mismatch of the outermost orbitals of S and C.[41] And the catalytic properties of N-doped carbon are attributed to the more positive charges on the surrounding C atoms due to the high electronegative of N atoms.[8] According to the density functional theory calculated by Qiao et al, when S and N are simultaneously incorporated into the carbon framework, it creates the high charge and spin densities of catalysts, thus leading to enhanced electrocatalytic performances for ORR.[42] Moreover, the Fe-based sites are also supposed to participate in the oxygen reduction at the same time. Therefore, it can be found that HPCFs, especially, HPCF-800, display the high ORR catalytic activity in alkaline media. HPCF-900 has the highest BET surface area, but its catalytic performance is lower than those of HPCF-800, maybe due to the relatively low contents of dopants S, N and Fe.

The stability of the catalysts and resistance to methanol crossover and CO poisoning effects are important consideration for their practical application to fuel cells. The stability of these catalysts was tested with under constant potentials for 10 h in O_2-saturated 0.1 M KOH aqueous solutions. From Figure 4a, it can be seen that the catalytic current density of HPCF-800 has decreased by 4% after 10 h of operation, while that of Pt/C decreased by 16% within the same period, indicating that a better stability of HPCF-800 than Pt/C catalyst. Based on the previous report,[42] its higher stability could be attributed to the strong strength of covalent heteroatom-carbon bonds in HPCF-800 and the improved chemical stability. The chronoamperometric responses to methanol introduced into an O_2-saturated 0.1 mol L^{-1} KOH solutions was also measured for HPCF-800 at a constant potential of −0.30 V. After the addition of 3 M methanol to electrolyte, the catalytic current density on the HPCF-800 modified GC electrode show subtle declination (Figure 4b). In contrast, the ORR current density for Pt/C catalysts decreases sharply by 89% (Figure 4b). As for the bubbling of CO, the catalytic current on HPCF-800/GC electrode decreased slowly to 90% while that of Pt/C sharply declined to 68% at the time of 450 s (Figure 4c). These results indicate that the HPCF-800 catalyst exhibits a high durability and good ability for avoiding methanol crossover effects and CO poisoning, thus having potential use in direct methanol fuel cells.

CONCLUSIONS

In summary, HPCFs ORR electrocatalysts with hierarchically porous structures were fabricated through pyrolysis of the as-prepared PEDOT-PSS aerogels. XPS and Raman analysis have demonstrated the S, trace N and Fe codoping in carbon framework in HPCFs, which serve as main active catalytic sites

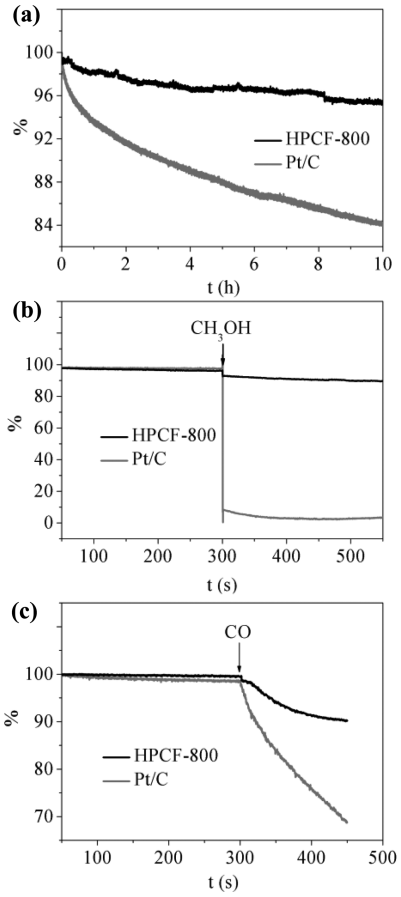

Figure 4. (a) Durability evaluation of Pt/C and HPCF-800 for 10 h in O_2-saturated 0.1 M KOH solutions at −0.3 V and a rotation rate of 800 rpm. (b, c) Chronoamperometric responses of Pt/C and HPCF-800 in O_2-saturated 0.1 M KOH solution at −0.3 V. The arrows indicate the introduction of 3 M methanol or CO.

for the effective oxygen reduction in the ORR process. Therefore, the high specific surface areas and hierarchically porous structures of the HPCFs, as well as the homogeneously distributed active sites, may enhance the ORR electrocatalytic performance of HPCFs catalysts. More importantly, the better methanol/CO tolerance than commercial Pt/C, combined with its long-term stability, make HPCFs as the promising low-cost metal-free electrocatalyst for practical application. The study presented here not only shows an example of low-cost and promising alternative to commercial Pt/C catalysts but also might be extended to preparation of other kinds of hierarchical porous carbon materials for wide applications.

■ ASSOCIATED CONTENT

Supporting Information

Molecular structures of PEDOT-PSS, SEM images of HPCF-700 and HPCF-900, nitrogen adsorption−desorption isotherms of PEDOT-PSS, HPCF-700, HPCF-800 and HPCF-900 with corresponding pore-size distributions, XPS elemental analyses of PEDOT-PSS, HPCF-700, HPCF-800 and HPCF-900, high resolution C 1s, N 1s, O 1s and Fe 2p spectra of PEDOT-PSS, HPCF-700, HPCF-800 and HPCF-900, TGA curve of PEDOT-PSS, CV curves of HPCF-700 and HPCF-900 and LSV and K-L plots of as-prepared PEDOT-PSS, HPCF-700 and HPCF-900. This material is available free of charge via the Internet at http://pubs.acs.org.

■ AUTHOR INFORMATION

Corresponding Author

*Y. Zhu. Fax: +86 10-82338212. E-mail: zhuying@buaa.edu.cn.

Notes

The authors declare no competing financial interest.

■ ACKNOWLEDGMENTS

The authors thank the financial support by the National Natural Science Foundation of China (51273008, 51473008), the National High-Tech Research and Development Program (2012AA030305), and the National Basic Research Program (2012CB933200).

■ REFERENCES

(1) Winter, M.; Brodd, R. J. What Are Batteries, Fuel Cells, and Supercapacitors? *Chem. Rev.* **2004**, *104*, 4245−4270.
(2) Shen, P. K.; Meng, H. The Beneficial Effect of the Addition of Tungsten Carbides to Pt Catalysts on the Oxygen Electroreduction. *Chem. Commun.* **2005**, 4408−4410.
(3) Liang, H. W.; Cao, X.; Zhou, F.; Cui, C. H.; Zhang, W. J.; Yu, S. H. A Free-Standing Pt-Nanowire Membrane as a Highly Stable Electrocatalyst for the Oxygen Reduction Reaction. *Adv. Mater.* **2011**, *23*, 1467−1471.
(4) Huang, H.; Liu, K.; Chen, K.; Zhang, Y.; Zhang, Y.; Wang, S.; Ce, F. Comodification on the Crystal Structure and Enhanced Photocatalytic Activity of Bi_2WO_6 Photocatalyst under Visible Light Irradiation. *J. Phys. Chem. C* **2014**, *118*, 14379−14387.
(5) Tian, N.; Zhang, Y.; Huang, H.; He, Y.; Guo, Y. Influences of Gd Substitution on the Crystal Structure and Visible-Light-Driven Photocatalytic Performance of Bi_2WO_6. *J. Phys. Chem. C* **2014**, *118*, 15640−15648.
(6) Paraknowitsch, J. P.; Zhang, Y.; Wienert, B.; Thomas, A. Nitrogen- and Phosphorus-Co-Doped Carbons with Tunable Enhanced Surface Areas Promoted by the Doping Additives. *Chem. Commun.* **2013**, *49*, 1208−1210.
(7) Yang, L.; Jiang, S.; Zhao, Y.; Zhu, L.; Chen, S.; Wang, X.; Wu, Q.; Ma, J.; Ma, Y.; Hu, Z. Boron-Doped Carbon Nanotubes as Metal-Free Electrocatalysts for the Oxygen Reduction Reaction. *Angew. Chem., Int. Ed.* **2011**, *50*, 7132−7135.
(8) Gong, K.; Du, F.; Xia, Z.; Durstock, M.; Dai, L. Nitrogen-Doped Carbon Nanotube Arrays with High Electrocatalytic Activity for Oxygen Reduction. *Science* **2009**, *323*, 760−764.
(9) Yang, L.; Jiang, S.; Zhao, Y.; Zhu, L.; Chen, S.; Wang, X.; Wu, Q.; Ma, J.; Ma, Y.; Hu, Z. Boron-Doped Carbon Nanotubes as Metal-Free Electrocatalysts for the Oxygen Reduction Reaction. *Angew. Chem., Int. Ed.* **2011**, *50*, 7132−7135.
(10) Gong, K.; Du, F.; Xia, Z.; Durstock, M.; Dai, L. Nitrogen-Doped Carbon Nanotube Arrays with High Electrocatalytic Activity for Oxygen Reduction. *Science* **2009**, *323*, 760−764.
(11) Zhang, L.; Niu, J.; Li, M.; Xia, Z. Catalytic Mechanisms of Sulfur-Doped Graphene as Efficient Oxygen Reduction Reaction Catalysts for Fuel Cells. *J. Phys. Chem. C* **2014**, *7*, 3545−3553.
(12) Liang, J.; Jiao, Y.; Jaroniec, M.; Qiao, S. Z. Sulfur and Nitrogen Dual-Doped Mesoporous Graphene Electrocatalyst for Oxygen Reduction with Synergistically Enhanced Performance. *Angew. Chem., Int. Ed.* **2012**, *51*, 11496−11500.
(13) Yu, D.; Xue, Y.; Dai, L. Vertically Aligned Carbon Nanotube Arrays Co-Doped with Phosphorus and Nitrogen as Efficient Metal-Free Electrocatalysts for Oxygen Reduction. *J. Phys. Chem. Lett.* **2012**, *3*, 2863−2870.
(14) Wang, S.; Zhang, L.; Xia, Z.; Roy, A.; Chang, D. W.; Baek, J. B.; Dai, L. BCN Graphene as Efficient Metal-Free Electrocatalyst for the Oxygen Reduction Reaction. *Angew. Chem., Int. Ed.* **2012**, *51*, 4209−4212.
(15) Choi, J.-Y.; Hsu, R. S.; Chen, Z. Highly Active Porous Carbon-Supported Nonprecious Metal−N Electrocatalyst for Oxygen

Reduction Reaction in Pem Fuel Cells. *J. Phys. Chem. C* **2010**, *114*, 8048−8053.
(16) Liang, H.-W.; Wei, W.; Wu, Z.-S.; Feng, X.; Müllen, K. Mesoporous Metal−Nitrogen-Doped Carbon Electrocatalysts for Highly Efficient Oxygen Reduction Reaction. *J. Am. Chem. Soc.* **2013**, *135*, 16002−16005.
(17) Liu, Z.; Zhang, G.; Lu, Z.; Jin, X.; Chang, Z.; Sun, X. One-Step Scalable Preparation of N-Doped Nanoporous Carbon as a High-Performance Electrocatalyst for the Oxygen Reduction Reaction. *Nano Res.* **2013**, *6*, 293−301.
(18) Wu, Q.; Xu, Y.; Yao, Z.; Liu, A.; Shi, G. Supercapacitors Based on Flexible Graphene/Polyaniline Nanofiber Composite Films. *ACS Nano* **2010**, *4*, 1963−1970.
(19) Yu, G.; Hu, L.; Liu, N.; Wang, H.; Vosgueritchian, M.; Yang, Y.; Cui, Y.; Bao, Z. Enhancing the Supercapacitor Performance of Graphene/MnO_2 Nanostructured Electrodes by Conductive Wrapping. *Nano Lett.* **2011**, *11*, 4438−4442.
(20) Xia, L.; Wei, Z.; Wan, M. Conducting Polymer Nanostructures and Their Application in Biosensors. *J. Colloid Interface Sci.* **2010**, *341*, 1−11.
(21) Groenendaal, L.; Jonas, F.; Freitag, D.; Pielartzik, H.; Reynolds, J. R. Poly (3, 4 - Ethylenedioxythiophene) and Its Derivatives: Past, Present, and Future. *Adv. Mater.* **2000**, *12*, 481−494.
(22) Bashyam, R.; Zelenay, P. A Class of Non-Precious Metal Composite Catalysts for Fuel Cells. *Nature* **2006**, *443*, 63−66.
(23) He, S.; Hu, X.; Chen, S.; Hu, H.; Hanif, M.; Hou, H. Needle-like Polyaniline Nanowires on Graphite Nanofibers: Hierarchical Micro/Nano-Architecture for High Performance Supercapacitors. *J. Mater. Chem.* **2012**, *22*, 5114−5120.
(24) Guo, Z.; Liu, H.; Jiang, C.; Zhu, Y.; Wan, M.; Dai, L.; Jiang, L. Biomolecule-Doped Pedot with Three-Dimensional Nanostructures as Efficient Catalyst for Oxygen Reduction Reaction. *Small* **2014**, *10*, 2087−2095.
(25) Guo, Z.; Qiao, Y.; Liu, H.; Ding, C.; Zhu, Y.; Wan, M.; Jiang, L. Self-Assembled Hierarchical Micro/Nano-Structured PEDOT as an Efficient Oxygen Reduction Catalyst over a Wide pH Range. *J. Mater. Chem.* **2012**, *22*, 17153−17158.
(26) Morozan, A.; Jégou, P.; Campidelli, S.; Palacin, S.; Jousselme, B. Relationship between Polypyrrole Morphology and Electrochemical Activity Towards Oxygen Reduction Reaction. *Chem. Commun.* **2012**, *48*, 4627−4629.
(27) Wu, G.; More, K. L.; Johnston, C. M.; Zelenay, P. High-Performance Electrocatalysts for Oxygen Reduction Derived from Polyaniline, Iron, and Cobalt. *Science* **2011**, *332*, 443−447.
(28) Xu, Y.; Sui, Z.; Xu, B.; Duan, H.; Zhang, X. Emulsion Template Synthesis of All Conducting Polymer Aerogels with Superb Adsorption Capacity and Enhanced Electrochemical Capacitance. *J. Mater. Chem.* **2012**, *22*, 8579−8584.
(29) Zhang, X.; Chang, D.; Liu, J.; Luo, Y. Conducting Polymer Aerogels from Supercritical Co2 Drying PEDOT-PSS Hydrogels. *J. Mater. Chem.* **2010**, *20*, 5080−5085.
(30) Zhao, Y.; Liu, B.; Pan, L.; Yu, G. 3D Nanostructured Conductive Polymer Hydrogels for High-Performance Electrochemical Devices. *Energy Environ. Sci.* **2013**, *6*, 2856−2870.
(31) Bai, H.; Sheng, K.; Zhang, P.; Li, C.; Shi, G. Graphene Oxide/Conducting Polymer Composite Hydrogels. *J. Mater. Chem.* **2011**, *21*, 18653−18658.
(32) Wei, H.; Xu, M.-W.; Bao, S.-J.; Yang, F.; Chai, H. Design and Synthesis of Carbonized Polypyrrole-Coated Graphene Aerogel Acting as an Efficient Metal-Free Catalyst for Oxygen Reduction. *RSC Adv.* **2014**, *4*, 16979−16984.
(33) Teng, C.; Lu, X.; Zhu, Y.; Wan, M.; Jiang, L. Polymer in Situ Embedding for Highly Flexible, Stretchable and Water Stable PEDOT:PSS Composite Conductors. *RSC Adv.* **2013**, *3*, 7219−7223.
(34) Montibon, E.; Lestelius, M.; Järnström, L. Electroconductive Paper Prepared by Coating with Blends of Poly(3,4-ethylenedioxythiophene)/Poly(4-styrenesulfonate) and Organic Solvents. *J. Appl. Polym. Sci.* **2010**, *117*, 3524−3532.
(35) Chu, P. K.; Li, L. Characterization of Amorphous and Nanocrystalline Carbon Films. *Mater. Chem. Phys.* **2006**, *96*, 253−277.
(36) Diaz, J.; Paolicelli, G.; Ferrer, S.; Comin, F. Separation of the sp^3 and sp^2 Components in the C1s Photoemission Spectra of Amorphous Carbon Films. *Phys. Rev. B* **1996**, *54*, 8064.
(37) Bottger-Hiller, F.; Mehner, A.; Anders, S.; Kroll, L.; Cox, G.; Simon, F.; Spange, S. Sulphur-Doped Porous Carbon from a Thiophene-based Twin Monomer. *Chem. Commun.* **2012**, *48*, 10568−10570.
(38) Paraknowitsch, J. P.; Thomas, A.; Schmidt, J. Microporous Sulfur-Doped Carbon from Thienyl-based Polymer Network Precursors. *Chem. Commun.* **2011**, *47*, 8283−8285.
(39) Antiohos, D.; Folkes, G.; Sherrell, P.; Ashraf, S.; Wallace, G. G.; Aitchison, P.; Harris, A. T.; Chen, J.; Minett, A. I. Compositional Effects of PEDOT-PSS/Single Walled Carbon Nanotube Films on Supercapacitor Device Performance. *J. Mater. Chem.* **2011**, *21*, 15987−15994.
(40) Yue, L.; Wang, S.; Zhao, X.; Zhang, L. Nano-Silicon Composites Using Poly(3,4-ethylenedioxythiophene):Poly(styrenesulfonate) as Elastic Polymer Matrix and Carbon Source for Lithium-Ion Battery Anode. *J. Mater. Chem.* **2012**, *22*, 1094−1099.
(41) Yang, Z.; Yao, Z.; Li, G.; Fang, G.; Nie, H.; Liu, Z.; Zhou, X.; Chen, X. a.; Huang, S. Sulfur-Doped Graphene as an Efficient Metal-Free Cathode Catalyst for Oxygen Reduction. *ACS Nano* **2011**, *6*, 205−211.
(42) Liang, J.; Jiao, Y.; Jaroniec, M.; Qiao, S. Z. Sulfur and Nitrogen Dual-Doped Mesoporous Graphene Electrocatalyst for Oxygen Reduction with Synergistically Enhanced Performance. *Angew. Chem., Int. Ed.* **2012**, *51*, 11496−11500.